Large-strain poro-elastoplastic axisymmetric analysis of boreholes

M. Kattis
Norwegian University of Science and Technology, Trondheim, Norway
michael.kattis@ntnu.no

E. Papamichos
Aristotle University of Thessaloniki – School of Civil Engineering, Thessaloniki, Greece, and SINTEF Industry, Trondheim, Norway

A. Lavrov
Norwegian University of Science and Technology, Trondheim, Norway

Abstract

The large strain behavior of materials is significant in various applications in geomechanics. This paper presents the formulation of a finite element model that implements material and geometric nonlinearities, as well as coupling with fluid flow through the porous medium. The model is applied on axisymmetric problems that are common in tunnels or boreholes. The material is assumed to be pressure dependent elastoplastic. Results are presented for a borehole under in situ isotropic stress. A large stress and pore pressure is applied to test the response in the large strain domain and the solution is compared with that predicted by small strain theory. The results demonstrate that large strain analysis provides a more realistic response above a certain strain.

1. Introduction

Boreholes and tunnels under isotropic in situ stresses are common structures that can be analyzed in an axisymmetric setting allowing the simplification of the analysis. There is a possibility that large deformations can arise in these problems and given the fact that geomaterials often may experience significant volumetric strains, the formulation of the elastoplastic process requires extra care. Finite element analysis can be utilized to obtain the solution of the coupled poroelastic and poroelastoplastic problem. Geometric nonlinearities arising from the solid's deformation render the standard problem fully coupled even when the permeability of the material is assumed independent of its deformation.

The elastic axisymmetric problem has been solved (Durban 1987) by quadratures. Durban uses the logarithmic ('Hencky') strain which is suitable for large strain analysis. However an assumption is made that the Cauchy (true) stress is computed directly from the product of Hencky strain and the elastic relations but this product should result in the Kirchoff stress instead (Xiao and Chen 2003). This assumption is correct when volumetric strains remain relatively small but ground materials may experience significant volumetric strains. The elastoplastic problem is solved (Papanastasiou and Durban 1997) by Durban and Papanastasiou for a Mohr-Coulomb and a Drucker-Prager yield function. Again the above assumption is utilized. (Vrakas and Anagnostou 2013) solve the

elastoplastic problem with a series approach. But the same assumption is also used and in addition the higher order terms of the elastic logarithmic strain are dropped to achieve an exact solution.

The goal of this study is to develop a framework for an elastoplastic porous medium in axisymmetric conditions that can be coupled to fluid flow in the large strain domain. The elastoplastic formulation is developed for the Cauchy (true) stress and not the Kirchoff stress since the former is more accurate.

2. Formulation of the stress – strain law in large strain

2.1 Hencky elasticity

In the cylindrical coordinate system r, θ, z of a vertical borehole and for plane strain conditions along the z-axis of the borehole and taking advantage of the axisymmetry along θ, the only remaining displacement is in the radial direction, i.e.

$$u_r \neq 0,\ u_z = 0,\ u_\theta = 0 \tag{1}$$

where u_r, u_θ, u_z are the radial, tangential and axial displacement, respectively.

In addition, for no variation along θ

$$\frac{\partial u_r}{\partial \theta} = 0 \tag{2}$$

Because of (1) and (2) the discretization can be carried out with 1 dimensional elements along the radial direction.

For axisymmetric plane strain conditions, the deformation gradient becomes

$$[F] = \begin{bmatrix} 1 + \dfrac{\partial u_r}{\partial R} & 0 & 0 \\ 0 & 1 + \dfrac{u_r}{R} & 0 \\ 0 & 0 & 1 \end{bmatrix} \tag{3}$$

where R is the radial coordinate in the initial configuration.

An appropriate measure of strain for large deformations is the logarithmic 'Hencky' strain (Durban 1987) (Papanastasiou and Durban 1997). The Hencky strain tensor is computed from the deformation gradient as

$$[\varepsilon_{tensor}] = \frac{1}{2}\ln(\,[F][F]^T\,) \tag{4}$$

and because the deformation gradient is diagonal, $[\varepsilon_{tensor}]$ reduces to

$$[\varepsilon_{tensor}] = \begin{bmatrix} \ln\left(1 + \dfrac{\partial u_r}{\partial R}\right) & 0 & 0 \\ 0 & \ln\left(1 + \dfrac{u_r}{R}\right) & 0 \\ 0 & 0 & 0 \end{bmatrix} \tag{5}$$

Therefore, $[\varepsilon_{tensor}]$ can be written in Voigt notation as:

$$\{\varepsilon_{voigt}\} = [\ \varepsilon_r \quad \varepsilon_\theta \quad 0\ ]^T \tag{6}$$

with $\varepsilon_r = \ln\left(1 + \frac{\partial u_r}{\partial R}\right)$, $\varepsilon_\theta = \ln\left(1 + \frac{u_r}{R}\right)$

In the following the subscript "Voigt" will be dropped and therefore, $\{\varepsilon\} = \{\varepsilon_{voigt}\}$

Hencky strain can capture the response in the large strain domain since it tends to negative infinity when large compressive deformations occur and at positive infinity when large tensile deformations occur.

To calculate the stress, a stress – strain law needs to be formulated. In this case a linear hyperelastic law is used for the elastic response. The elasticity matrix for plane strain conditions is given as

$$[C^e] = \frac{E}{(1+\nu)(1-2\nu)}\begin{bmatrix} 1-\nu & \nu & \nu \\ \nu & 1-\nu & \nu \\ \nu & \nu & 1-\nu \end{bmatrix} \tag{7}$$

where C^e is elastic stiffness matrix, and E, ν are the Young's modulus and Poisson's ratio respectively. For axisymmetric problems the shear stresses are zero and therefore the relevant rows and columns are omitted in the stiffness matrix. The Hencky strain is energy conjugate to the Kirchhoff effective stress τ' (e.g., Xiao and Chen 2003). Thus, for an elastic material the following relationship holds

$$\{\tau'\} = [C^e]\{\varepsilon\} \tag{8}$$

with $\{\tau'\} = [\ \tau_r'\ \ \tau_\theta'\ \ \tau_z'\ ]^T = \mathcal{J}\{\sigma'\}$, $\{\sigma'\} = [\ \sigma_r'\ \ \sigma_\theta'\ \ \sigma_z'\ ]^T$

$\mathcal{J} = \det[F] = \left(1 + \frac{\partial u_r}{\partial R}\right)\left(1 + \frac{u_r}{R}\right)$

where σ_r' , σ_θ' , σ_z' radial, angular and vertical Cauchy (true) stress.

The total Kirchoff stress used for the calculation of the finite element components is written as

$$\{\tau\} = \{\tau\}' - \mathcal{J}p_f\{I\} \tag{9}$$

where p_f pore fluid pressure computed from the fluid phase

$\{I\} = [1\ \ 1\ \ 1]^T$ is the unit vector.

2.2. Elastoplasticity

The stress computation in the elastoplastic regime is based on the multiplicative decomposition of the deformation gradient into a plastic and elastic part. Using an exponential return map algorithm along with the logarithmic strain measure the return map algorithm reduces to a small strain equivalent (Meschke and Liu 1999). Defining $\{\sigma_0'\}$ as the Cauchy effective stress at the beginning of the increment and assuming only the elastic part of the deformation gradient causes a change in stress, the elastic part of the deformation gradient at the beginning of the increment can be computed as

$$[F_0^e] = \begin{bmatrix} \exp({}_0\varepsilon_r^e) & 0 & 0 \\ 0 & \exp({}_0\varepsilon_\theta^e) & 0 \\ 0 & 0 & \exp({}_0\varepsilon_z^e) \end{bmatrix} \tag{10}$$

with $[{}_0\varepsilon_r^e\ \ {}_0\varepsilon_\theta^e\ \ {}_0\varepsilon_z^e]^T = \mathcal{J}_0[C^e]^{-1}\{\sigma_0'\}$, $\mathcal{J}_0 = \det[F_0]$

And from the multiplicative decomposition:

$$[F_0] = [F_0^e]\,[F_0^p] \;\Rightarrow\; [F_0^p] = [F_0^e]^{-1}[F_0] \tag{9}$$

where $[F_0]$, $[F_0^p]$ total and plastic deformation gradients at the beginning of the increment.

In order for the algorithm to be initiated a trial elastic strain needs to be defined. To do so it is assumed that the whole increment is elastic and therefore, the whole increment of the total deformation gradient is applied on $[F_0^e]$ to compute the trial elastic deformation gradient.

$$[F_{trial}^e] = [\Delta F][F_0^e] \tag{12}$$

where $[\Delta F]$ the total deformation gradient increment.
$[F_{trial}^e]$ trial elastic deformation gradient.

Finally the elastic trial strain $\{\varepsilon_{trial}^e\}$ is computed from equations (4,5,6) using $[F_{trial}^e]$ instead of $[F]$.

For large volumetric strains, $\mathcal{J} \neq 1$ and it is inaccurate to assume that the yield criterion is a function of the Kirchoff stress. Therefore, the yield and plastic potential functions are formulated with the Cauchy effective stress. The trial Cauchy stress is computed from the elastic trial strain as:

$$\{\sigma'_{trial}\} = \frac{C_e\{\varepsilon_{trial}^e\}}{\mathcal{J}} \tag{13}$$

Defining $f(\{\sigma'\}, \kappa)$, $g(\{\sigma'\}, \kappa)$, $p(\{\sigma'\}, \kappa)$ as the yield function, plastic potential and hardening function, respectively, with κ being the hardening variable, the algorithm to update the stress proceeds as follows.

A check on whether the trial stress violates the yield function is performed.

$$f(\{\sigma'_{trial}\}, \kappa_0) \leq 0 \tag{14}$$

If the condition is fulfilled the step is elastic and the algorithm exits and the updated stress is the trial stress. If the condition is violated, then the following algebraic equations of the backwards Euler scheme must be solved for the unknown variables $\sigma', \Delta\lambda, \varepsilon_e, \kappa$ (Meschke and Liu 1999)

$$\{\sigma'\} = \frac{[C_e]\{\varepsilon^e\}}{\mathcal{J}} \tag{15}$$

$$\mathcal{J}(\{\varepsilon_e\} - \{\varepsilon_{trial}^e\}) = \Delta\lambda \frac{\partial g}{\partial\{\sigma'\}} \tag{16}$$

$$\kappa - \kappa_0 = \Delta\lambda p(\{\sigma'\}, \kappa) \tag{17}$$

$$f(\{\sigma'\}, \kappa) = 0 \tag{18}$$

where $\Delta\lambda$ is the plastic multiplier, κ_0 the initial value of the hardening variable and ε_e is the elastic strain.

3 . Finite element formulation

For the global solid problem a total Lagrangian formulation is employed. The internal element force vector f_{int}, with the Kirchoff stress is computed as

$$\{f_{int}\} = \int_{R_a}^{R_b} [B^T] \begin{Bmatrix} \tau_r \\ \tau_\theta \end{Bmatrix} R \, dR \tag{19}$$

where B^T the strain - displacement matrix derived with respect to the initial configuration
R_a , R_b undeformed element left and right radial nodal coordinates.

$[B]$ is computed as (Heidi Igland Jacobsen 2021)

$$[B] = [B_L][B_0] \tag{20}$$

with

$$[B_L] = \begin{bmatrix} 1 + \left\{\frac{\partial N}{\partial R}\right\}^T \{U\} & 0 \\ 0 & 1 + \frac{\{N\}^T\{U\}}{R} \end{bmatrix}, \quad [B_0] = \begin{bmatrix} \frac{\partial N_1}{\partial R} & \frac{\partial N_2}{\partial R} & \cdots \\ \frac{N_1}{R} & \frac{N_2}{R} & \cdots \end{bmatrix} \tag{21}$$

where N_i is the element shape function of the i_{th} element node and N , U the vector of element shape functions and nodal displacements respectively.

We solve the coupled problem using an iterative scheme resembling a fixed-point iteration. For each increment the solid phase is solved assuming the fluid phase is frozen and vice – versa. Then both the fluid and solid phases are solved again with the updated values of each other until convergence is reached. The scheme can be written in this way.

$$\{U_{i+1}\} = \{U_0\} + \{\Delta U(P_i)\} \tag{22}$$

$$\{P_{i+1}\} = f_{fluid}(\{U_{i+1}\}) \tag{23}$$

where P , U are the global pore pressure and displacement vectors, subscript i denotes the iteration number and ΔU , f_{fluid} represent an iteration in the solid phase and in the fluid phase respectively. The convergence criterion is:

$$\frac{|\Delta U(P_i)|}{|\Delta U(P_0)|} < 0.001 \ \ and \ \ \frac{|P_i - P_{i-1}|}{|P_1 - P_0|} < 0.001 \tag{24}$$

Both conditions of (24) need to be fulfilled for the algorithm to exit. The scheme appears to converge for both the elastic and elastoplastic case.

4. Results

In the analyzed problem the borehole is loaded externally by an external stress σ_e and a pore fluid pressure p_e at a far field radius R_e while the borehole with internal radius R_i is free from load and pore fluid pressure, as shown schematically in Figure 1. An external radius 10 times the internal radius is used in the simulations.

The material is assumed to be elastic perfectly plastic with a Drucker – Prager yield criterion and a non associative flow rule. The equations for the yield criterion and plastic potential are:

$$f(\{\sigma\}') = \sqrt{J_2} + B_\phi I_1 - A \ , \ \ g(\{\sigma\}') = \sqrt{J_2} + B_\psi \tag{25}$$

where $A = \frac{6c\cos\phi}{\sqrt{3}\,(3+\sin\phi)}$, $B_\phi = \frac{2\sin\phi}{\sqrt{3}\,(3+\sin\phi)}$, $B_\psi = \frac{2\sin\psi}{\sqrt{3}\,(3+\sin\psi)}$

$I_1 = \sigma'_r + \sigma'_\theta + \sigma'_z$

$J_2 = \frac{1}{6}[(\sigma'_r - \sigma'_\theta)^2 + (\sigma'_r - \sigma'_z)^2 + (\sigma'_\theta - \sigma'_z)^2]$

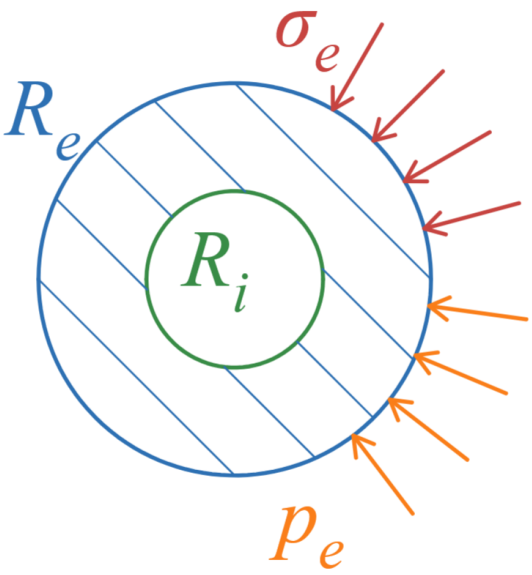

Fig. 1. Schematic of a horizontal section of a borehole with the applied external load and pore pressure..

with parameters:

$$\phi = 29°\,,\ \ \psi = 3°\ ,\ \ c = \frac{E}{300} \tag{26}$$

where ϕ , and ψ are the internal friction and dilatancy angles, respectively, and c is the cohesion.

Large deformations are obtained by reaching a relatively large external stress and pore pressure, i.e.

$$\sigma_e = 0.5E\,,\ \ p_e = 0.05E \tag{27}$$

It is important for this excessive deformation to occur so that the algorithm can be tested and compared for the small strain analysis.

Figure 2 presents the external stress versus the cavity radial deformation. The stress is normalized with the Young's modulus and the deformation with the initial internal radius.

The plot for large strains is compared with the response of the small strain analysis with the same parameters. The two plots coincide with each other for small deformations. However, after the load becomes large the response predicted from small strain theory is not reasonable since the hole vanishes without any increase in stiffness. In contrast, the analysis with the large deformation theory predicts a much more realistic response since as the hole shrinks the structure becomes infinitely stiff. As a result, the point where the entire hole vanishes is approached asymptotically.

Figure 3 presents the stress radial profiles for the small strain and large strain case at a low stress $\sigma_e' = 0.033E$ and for a stress $\sigma_e' = 0.15E$ that is close to the maximum that is reached for the small strain analysis. The large strain results are plotted with the coordinates of the updated configuration while for the small strains the coordinates of the initial configuration are used. In both cases the radial coordinate is normalized with respect to the initial internal radius R_i. Again we see similar curves for small and large strains at the low stress. The profiles differ quite substantially for the larger stress.

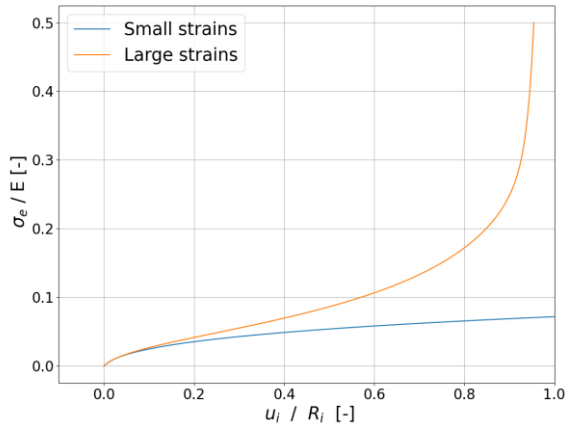

Fig. 2 Cavity closure curve for the external stress vs cavity radial deformation normalized by the Young's modulus and initial cavity radius, respectively, for small and large strain analysis.

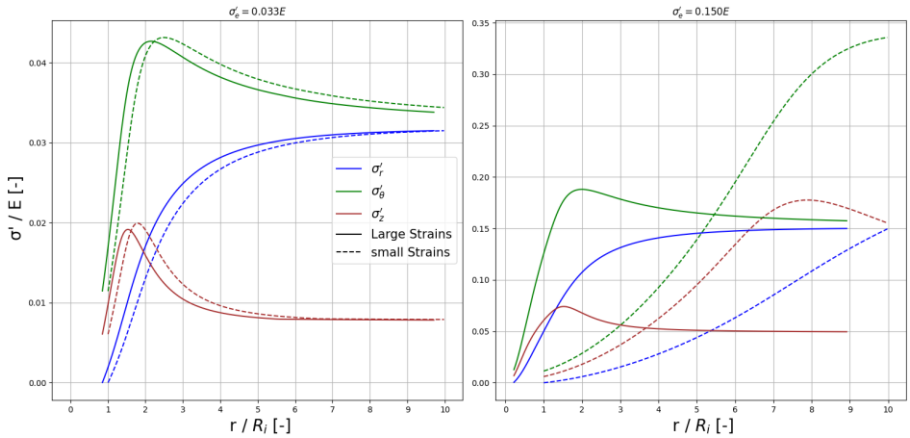

Fig. 3. Cauchy effective stress radial profiles for the small and large strain analysis for stress level of $\sigma'_e / E =$ 0.033 and 0.15. The large strain curves are plotted with the radial coordinate of the current configuration normalized by the initial internal radius. The small strain curves are plotted with the coordinates of the initial configuration.

Finally in Figure 4 the radial pore pressure profile is plotted for the final step of the large strain analysis. For comparison the pore pressure profile of an undeformed configuration is also presented. Both are plotted with respect to the initial coordinates which are normalized again by the internal initial radius. Because displacements are bigger towards the internal radius, we see a big difference for the two profiles. For this reason if displacements (not necessarily strains) are large the fully coupled problem should be solved.

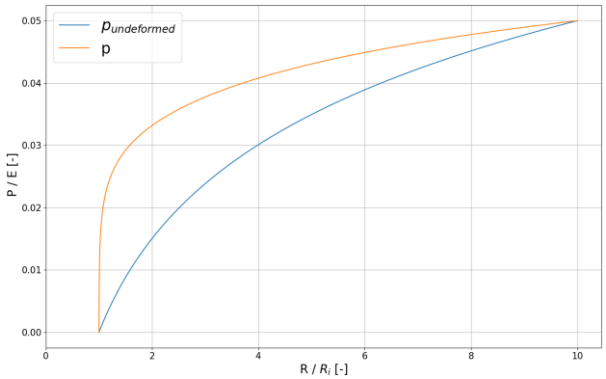

Fig 4 Pore pressure profiles for the deformed and undeformed configuration. The curves are plotted with the initial coordinates normalized with the initial internal radius.

5. Conclusions

A large-strain elastoplastic analysis for axisymmetric problems has been presented that is fully coupled with the pore fluid problem. The analysis employs a pressure dependent elastoplastic yield surface and uses the Cauchy stress as the input of the yield function and plastic potential. A comparison between a small strain solution is made and we can conclude that for the small strain range the small and large strain solutions coincide. However, in the large strain range the small strain solution stops giving reasonable results. Further work can target the implementation of different constitutive laws more complex than the Drucker – Prager model, as well as materials which have permeability varying with the deformation in 2d and 3d analysis.

6 . Acknowledgments

This work has been supported by the research project “Chalk influx and solids production mitigation in the North Sea” funded by the Research Council of Norway and Aker BP, ConocoPhillips Norway, and Hess Denmark (Petromaks 2 program, Project number 306106, 2020).

7 . References

Heng Xiao, Liang-Sen Chen (2003) Hencky’s logarithmic strain and dual stress–strain and strain–stress relations in isotropic finite hyperelasticity. International Journal of Solids and Structures Volume 40, (Issue 6): Pages 1455-1463. https://doi.org/10.1016/S0020-7683(02)00653-4 .

G. Meschke, W.N. Liu (1999) A re-formulation of the exponential algorithm for finite strain plasticity in terms of cauchy stresses. Computer Methods in Applied Mechanics and Engineering Volume 173 (Issues 1–2): Pages 167-187. ISSN 0045-7825. https://doi.org/10.1016/S0045-7825(98)00267-9.

Heidi Igland Jacobsen, Maren Eriksen Eia (2021) 2D Triangular Finite Elements based on Assumed Natural Coordinate Strains and the Seth-Hill Family of Finite Strains. Master thesis, Norwegian University of Science and technology - Institutt for maskinteknikk og produksjon

D. Durban (1988) A finite strain axially-symmetric solution for elastic tubes. International Journal of Solids and Structures Volume 24, (Issue 7): Pages 675-682. ISSN 0020-7683 https://doi.org/10.1016/0020-7683(88)90016-9 .

P. Papanastasiou, D. Durban (1997) ELASTOPLASTIC ANALYSIS OF CYLINDRICAL CAVITY PROBLEMS IN GEOMATERIALS. International Journal for Numerical and Analytical Methods in Geomechanics Volume 21, (Issue 2): Pages 133-149. https://doi.org/10.1002/(SICI)1096-9853(199702)21:2<133::AID-NAG866>3.0.CO;2-A

A. Vrakas, G. Anagnostou (2014), A finite strain closed-form solution for the elastoplastic ground response curve in tunnelling. International Journal for Numerical and Analytical Methods in Geomechanics Volume 38, (Issue 11) : Pages 1131-1148. https://doi.org/10.1002/nag.2250